Synthetic Metals 290 (2022) 117139

Contents lists available at ScienceDirect

Synthetic Metals

journal homepage: www.elsevier.com/locate/synmet

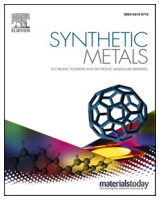

Novel 2,6-dimethoxyphenoxy alpha substituted phthalocyaninato metal complexes: Electrochemistry, *In situ* spectroelectrochemistry and oxygen electrocatalysis

Efe Baturhan Orman [a], Zuhal Yazar [a], Mehmet Pişkin, Co-Author [b], Zafer Odabaş [a,*], Ali Rıza Özkaya [a,*]

[a] Department of Chemistry, Marmara University, Kadıköy, 34722 Istanbul, Turkey
[b] Çanakkale Onsekiz Mart University, Vocational School of Technical Sciences, Department of Food Processing, 17100 Çanakkale, Turkey

ARTICLE INFO

Keywords:
Phthalocyanine
Aggregation
Dimethoxyphenoxy
Electrochemistry
Electrocatalysis
Oxygen reduction

ABSTRACT

Non-peripherally tetra-2,6-dimethoxyphenoxy substituted Co(II) **3**, Fe(II) **4**, Mn(III) **5**, and Ni(II) **6** phthalocyanines were prepared by refluxing the n-pentanol solution of their metal-free analogue H_2Pc **2**, (obtained by using 3-(2,6-dimethoxyphenoxy)phthalonitrile), metal salts ($Co(CH_3COO)_2.4\ H_2O$, $Fe(CH_3COO)_2$, $Mn(CH_3COO)_2.4\ H_2O$ or $NiCl_2$) and 1,8-diazabicyclo[5.4.0]undec-7-ene(DBU) as the catalyst under N_2 atmosphere for 2 h. The molecular structure of metallophthalocyanines **3–6** were explained by common methods which are elemental analysis, MALDI-TOF mass, FTIR, and UV-*Vis* spectroscopies. The complexes are well dissolved in various solvents (dichloromethane, tetrahydrofuran, dimethylsulfoxide, dimethylformamide, and toluene. Electrochemical redox, electrocatalytic oxygen reducing and electrocolorimetric properties of the phthalocyanine complexes were also measured by voltammetric and *in situ* UV-*Vis* spectroelectrochemical techniques. The phthalocyanine complexes displayed highly reversible sequential one-electron redox processes occurring at metal and/or phthalocyanine ring. The association of these processes with net colour changes pointed out their functionality as electrochromic material. Furthermore, the phthalocyanine complexes **3**-**5** and especially Fe(II)Pc **4**, showed striking electrocatalytic oxygen reducing activity, owing to the metal centres with redox activity, increasing their interplay with the O_2 molecule.

1. Introduction

In recent years, because of their thermal and chemical stability, convenience of modification, and unique optical and physicochemical properties, metallophthalocyanines (MPcs) have been attracting broad interest of the researchers, and thus, finding applicability in various fields of technology [1]. Chemical and electrochemical sensors [2,3], fibrous installations [4,5], nanostructured kit arranging and synthetically light antenna in solar energy system [6–8], photodynamic therapy [9], nonlinear optic [10], electrocatalysis [11], photocatalytic and photoelectrocatalytic hydrogen production [12] are among numerous areas of exploration and technology in which MPcs have been used. The chemical and the physical properties of MPcs can be changed by modifying the metal atom that centred in the complexes and/or non-peripheral and/or the peripheral substituents in phthalocyanine (Pc) complexes or axial ligands in the central metal atom [13,14]. The easy modification of this class of compounds guarantees their usability in the mentioned technological areas since an MPc should have specific properties for each area [15]. For instance, possessing rich electrochemical redox or electron transfer properties is highly critical for applicability in the areas of electrochemical sensors, electrochromism, and electrocatalysis, especially for electrochemical energy conversion and storage systems [16,17]. This can be achieved by placing different central metals, especially the ones behaving as redox-active, in the MPc molecule since Pc ring can also transfer electrons. Therefore, MPcs with tuneable redox and catalytic activity have received great attention in recent years as electrocatalysts for oxygen reduction reaction (ORR) [18–20]. On the other hand, for the development of MPc electrocatalysts possessing high performance, there is still serious problems such as the high overpotential and demetallation of the Pc ring centre [19].

Solubility also plays a critical role in ensuring technological applicability of MPcs . For instance, well dispersion of an MPc in the catalyst

* Corresponding authors.
E-mail addresses: mehmetpiskin@comu.edu.tr (M. Pişkin), zodabas@marmara.edu.tr (Z. Odabaş), aliozkaya@marmara.edu.tr (A.R. Özkaya).

https://doi.org/10.1016/j.synthmet.2022.117139
Received 8 May 2022; Received in revised form 4 July 2022; Accepted 8 July 2022
Available online 18 July 2022

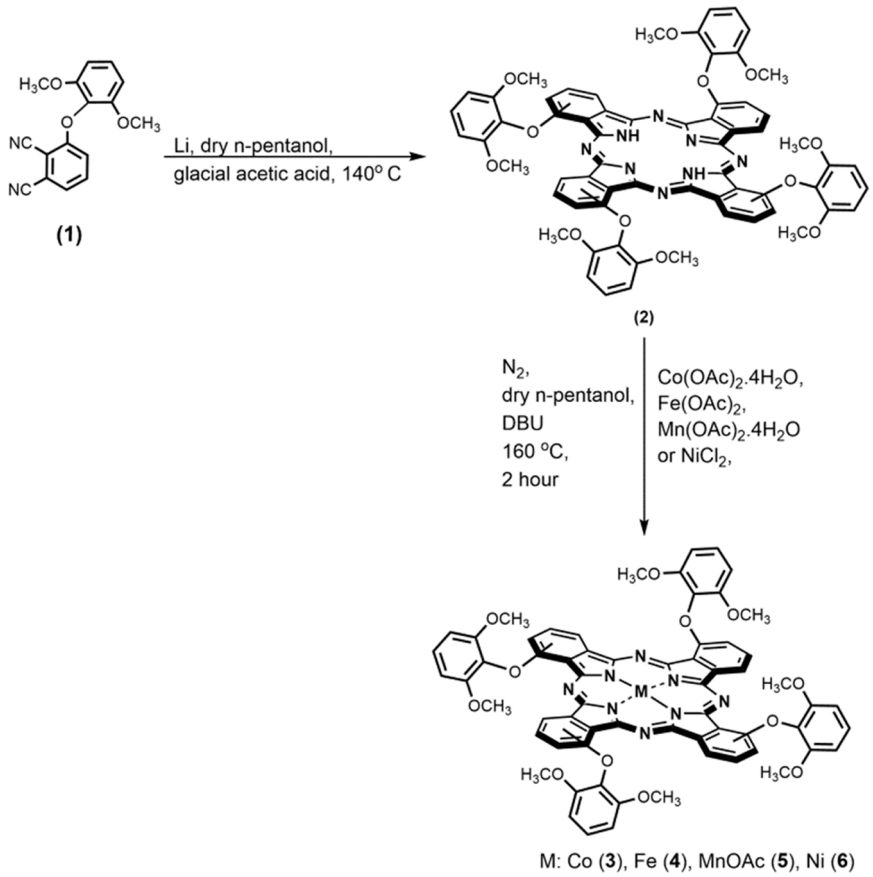

Scheme 1. Synthesis of non-peripherally 2,6-dimethoxyphenoxy substituted metallo phthalocyanine (3-6) derivatives.

surface is very important to be able to obtain its maximum catalytic activity. This can be achieved if the MPc shows high solubility in the solvent, used to prepare the catalyst ink. Unfortunately, it is common knowledge that because of the extended π system, Pcs may compose bulkier and more intricate aggregates and dimerize and the relevant intermolecular interactions reduce their solubility. Typically, a decline of the absorbance of the Q band belongs to monomeric species caused by Pc aggregation; in addition, it is also observed that the absorbance of a novel expansive blue shifted band rose. While shifting to blue (shorter wavelengths) belongs to H-type aggregates, longer wavelengths (red-shifted) band caused by the existence of J-aggregated species [21]. Fortunately, the substitution of appropriate groups on the macrocycle structure of Pc and metal centred in the Pc core enhances the solubility of these compounds [14,22].

In fact, the synthesis, electrochemical, spectroelectrochemical and the electro-catalytic dioxygen reduction properties of periferal substituted structural isomers of the starting and Pcs synthesized in this study were investigated in our previous study [23]. However, as many Pc researchers do, this study also contains with the synthesis, and structural characterization of novel MPcs with non-peripheral alkoxy substituents [24,25]. These Pc complexes displayed great solubility in various organic solvents (such as toluene, $CHCl_3$, dichloromethane (DCM), tetrahydrofuran (THF), dimethylformamide (DMF), and dimethylsulfoxide (DMSO)) like peripheral analogues. In addition, various central metals (Ni(II), Co(II), Mn(III) and Fe(II)) were placed in the centre in order to enrich the electron transfer properties (Scheme 1). Structural characterization of the newly synthesized Pc complexes with classical spectroscopic techniques was followed by a complete description of their electrochemical, electrochromic and electrocatalytic oxygen reducing features with the combined use of classical voltammetric and modern *in situ* spectroelectrochemical and hydrodynamic rotating electrode techniques. The metal-centered cores of the Pcs synthesized in this study are quite rich in electrons compared to their peripheral analogues. Because both the electron-donating methoxy groups in the outer ring and the electron-donating dimethoxyphenoxy groups in the inner ring are located in the ortho position. Since the ortho and para positions in the benzene ring are the locations where electron releasing and withdrawing are maximum, these Pc complexes have performed much superior properties than their peripheral analogues in applications related to electron transfer.

2. Experimental

Materials and equipments for synthesis were given in the supplementary information section.

2.1. Synthesis of alpha 2,6-dimethoxyphenoxy substituted phthalocyanine (H2Pc) (2)

0.12 g (0.43 mmol) 3-(2,6-dimethoxyphenoxy)− 1,2-dicyanobenzene (**1**), 15 ml of dry amyl alcohol 48 mg of granular lithium were stirred under reflux in a nitrogen atmosphere at 140 °C for 20 min. The desired alpha 2,6-dimethoxyphenoxy substituted metal free Pc product, H_2Pc (**2**) was obtained and cleansed by column chromatography by using silica gel, chloroform ($CHCl_3$): methanol (MeOH) (9:1) solvent system as an eluent according to literature[26]. Yield: 49.32 mg (41.1%). Due to the synthetic method used in this work, the yield of **2** was remarkably higher than that reported in the literature(18.0%) [26].

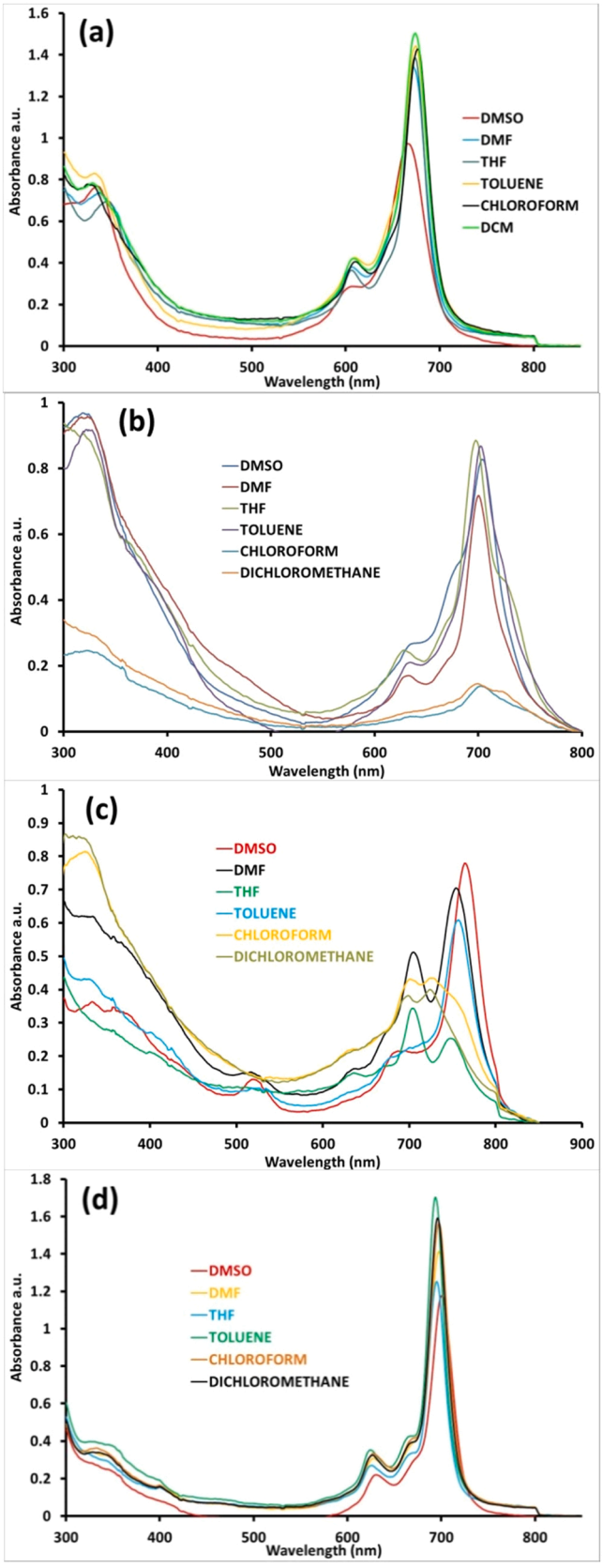

Fig. 1. Absorption spectra of the substituted CoPc 3 (a), FePc 4 (b), Mn(OAc)Pc 5 (c) and NiPc 6 (d) at 1.00×10^{-5} M in different solvents.

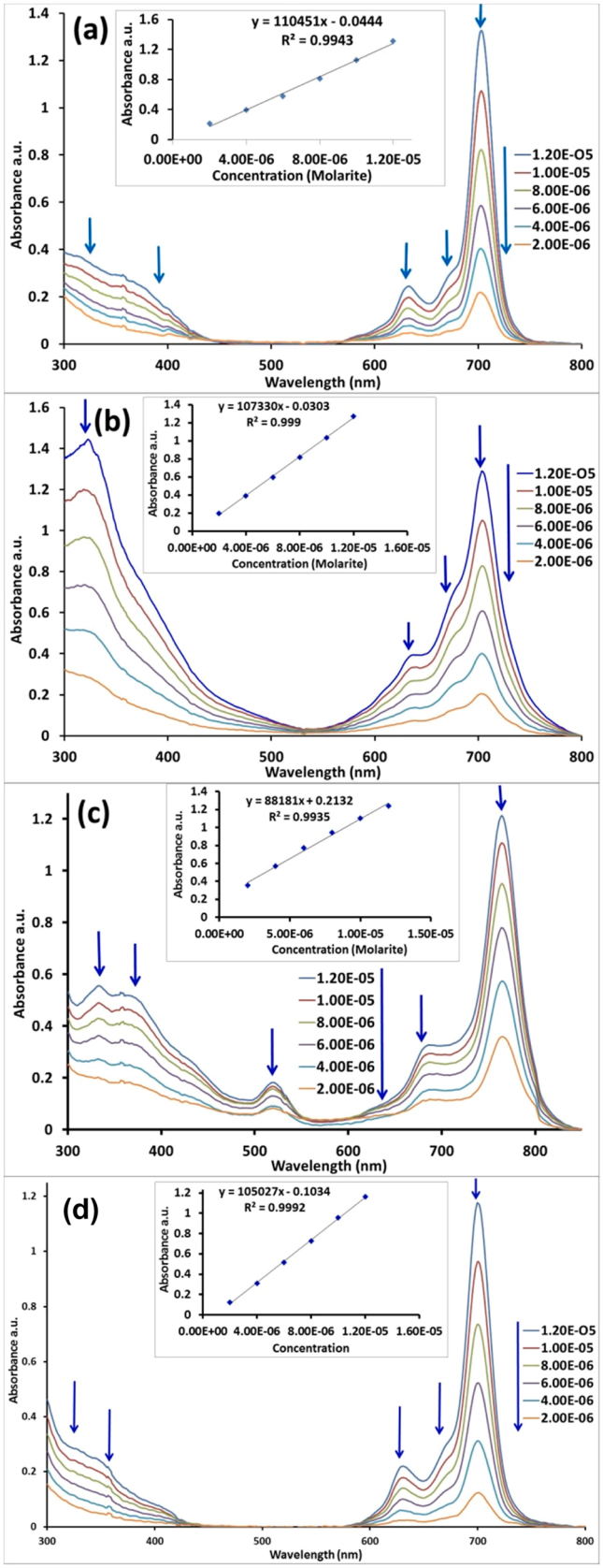

Fig. 2. Absorption spectra of CoPc 3 (a), FePc 4 (b), Mn(OAc)Pc 5 (c) and NiPc 6 (d) in DMSO at different concentrations. (inset: plot of absorbance vs. concentration).

Table 1
Electrochemical redox data for metal phthalocyanine complexes 3–6 in TBAP/DMSO and comparison with some analogues from literature and previously reported beta substituted ones [31]. All Potentials were referenced against SCE and recorded at 0.100 Vs^{-1} scan rate.

Oxidations Reductions								
Complex		Ring	M^{III}/M^{II}	M^{II}/M[a]	1st ring	2nd[b] ring	3r[b] ring	[b]$\Delta E_{1/2}$	Ref.
3	[c]$E_{1/2}$ (V)	*0.86*[d]	*0.36 (0.51)*[e]	*-0.49*	*-1.46*	–	–	*0.85*	*tw*[f]
CoPc	[g]ΔE_p (V)	–	*0.070 (0.065)*	*0.060*	*0.060*				
	[h]I_{pa}/I_{pc}	–	–	*0.96*	*0.88*				
β – CoPc	[c]$E_{1/2}$ (V)	*0.96*	*0.39*	*-0.48*	*-1.44*				[31]
4	[c]$E_{1/2}$ (V)	*0.58*[d]	*-0.58*	*-0.89*	*-1.38*		–	*1.16*	*tw*[f]
FePc	[g]ΔE_p (V)	–	*0.090*	*0.120*	*0.10*				
	[h]I_{pa}/I_{pc}	–	*0.92*	*0.90*	*0.94*				
β – FePc	[c]$E_{1/2}$ (V)	*0.96*	*-0.20*	*-0.80*	*-1.30*				[31]
5	[c]$E_{1/2}$ (V)	*0.92*[d]	*-0.22*	*-0.85*	*-1.55*	–	–	*1.14*	*tw*[f]
Mn(OAc)Pc	[g]ΔE_p (V)	–	*0.080*	*0.080*	*0.120*				
	[h]I_{pa}/I_{pc}	–	*0.95*	*0.94*	*0.84*				
β – Mn(OAc)Pc	[c]$E_{1/2}$ (V)	*0.95*	*-0.19*	*-0.81*	*-1.52*				[31]
6	[c]$E_{1/2}$ (V)	*0.75*	–	–	*-0.74*	*-1.27*	*-1.55*	*1.49*	*tw*[f]
NiPc	[g]ΔE_p (V)	*0.090*			*0.060*	*0.120*	*0.08*		
	[h]I_{pa}/I_{pc}	*0.90*			*0.94*	*0.88*	*0.90*		
β – NiPc	[c]$E_{1/2}$ (V)	*0.91*	–	–	*-0.79*	*-1.25*	–		[31]
CoPc	[c]$E_{1/2}$ (V)		*0.78*	*-0.39*	*-1.40*				[38][i]
FePc	[c]$E_{1/2}$ (V)		*0.51*	*-0.63*	*-1.05*				[28][i]
MnPc	[c]$E_{1/2}$ (V)		*-0.005*	*-0.70*	*-1.47*				[39][j]
CoPc	[c]$E_{1/2}$ (V)			*-0.37*	*-1.40*	*-1.80*			[14,35]
FePc	[c]$E_{1/2}$ (V)		*0.46*	*-0.71*	–				[14]
MnPc	[c]$E_{1/2}$ (V)		*-0.08*	*-0.75*	–				[14,37]

[a] The elecrochemical parameters of iron phthalocyanine, carrying 4-(4-methoxyphenyl)− 8-methyl-coumarin-7-oxy substituents at non-peripheral positions.
[b] $\Delta E_{1/2} = E_{1/2}$(first oxidation)-$E_{1/2}$ (first reduction). This value corresponds to the HOMO-LUMO gap for MPc complexes including a redox-active metal center, but to the charge transfer energies from metal to ligand or ligand to metal for MPc complexes involving a redox-active metal center.
[c] $E_{1/2} = (E_{pa}+E_{pc})/2$ at 0.10 V s^{-1}.
[d] These redox couples could be detected only by square wave voltammetry.
[e] The redox behaviour of the compounds was complicated by aggregation phenomenon and thus, some redox couples were split.
[f] this work.
[g] $\Delta E_p = E_{pa}-E_{pc}$ at 0.10 V s^{-1}.
[h] I_{pa}/I_{pc} for reduction, I_{pc}/I_{pa} for oxidation processes at 0.10 Vs^{-1} scan rate.
[i] The elecrochemical parameters of cobalt phthalocyanine, carrying 7-oxy-3-biphenylcoumarin substituents at non-peripheral positions.
[j] The elecrochemical parameters of manganese phthalocyanine, carrying dimethyl 5-oxyisophthalate substituent at peripheral positions.

2.2. General procedure for the synthesis of alpha 2,6-dimethoxyphenoxy substituted phthalocyaninato metal complexes (3-6)

In dry n-pentanol, the H_2Pc (**2**) (30.33 mg, 0.027 mmol) was heated by using excess 0.054 mmol of metal salts [13.45 mg $Co(OAc)_2.4\ H_2O$, 9.39 mg $Fe(OAc)_2$, 13.23 mg $Mn(OAc)_2.4\ H_2O$ or 7.00 mg $NiCl_2$] and 0.2 ml of DBU for 2 h at 150 °C. The reaction mixture was cooled and diluted with 10 ml of ethanol to precipitate the crude product. The suspension mixture was filtered in vacuo and the solids were washed with water, hot ethanol, methanol and acetone. The products were cleansed by using silica gel on column chromatography via $CHCl_3$: MeOH (9:1) solvent system as eluent. The products were more cleansed by using silica gel via solely THF solvent as eluent. The Pcs complexes were then dried under vacuum.

2.2.1. 1(4),8(11),15(18),22(25)-Tetrakis-(2,6-dimethoxyphenoxy) phthalocyaninato cobalt(II) (3)

The CoPc (**3**) is soluble in toluene, acetonitrile, $CHCl_3$, DCM, THF, DMF, and DMSO. Mp > 300° C. Yield: 9.64 mg (30.2%). Calculated for $C_{64}H_{48}CoN_8O_{12}$: C, 65.14%; H, 4.10%; N, 9.50%; found C, 64.99%; H, 4.24%; N, 9.65%. FTIR (ATR) λ_{max}/cm^{-1}: 893, 962, 1078(C—C str.), 1139(C—N str.), 1214(C—N str.), 1235(C—O str.), 1337(C—O str.), 1444, 1487(C—H bend.), 1605(C═C str.), 1658(C═N str.), 2848(>CH_2 str.), 2934(>CH_2 str.), 3013(=C—H str.), 3063(=C—H str.). UV–*Vis* (DMSO, 1 $\times 10^{-5}$ M): λ_{max}(nm), (log ε): 319 (4.64), 622 (4.15), 661 (4.20), 666 (4.99). MS *(*MALDI-TOF*) m/z* : calc.: 1180.07; found: 1181.13 $[M+H]^+$, 1198.13 $[M+H_2O]^+$.

2.2.2. 1(4),8(11),15(18),22(25)-Tetrakis-(2,6-dimethoxyphenoxy) phthalocyaninato iron(II) (4)

The FePc (**4**) is soluble in toluene, $CHCl_3$, DCM, THF, DMF, and DMSO. Mp > 300° C. Yield: 7.46 mg (23.5%). Calculated for $C_{64}H_{48}FeN_8O_{12}$: C, 65.31%; H, 4.11%; N, 9.52%; found C, 65.19%; H, 4.23%; N, 9.64%. FT-IR (ATR) λ_{max}/cm^{-1}: 875, 971, 1072(C—C str.), 1113(C—N str.), 1190(C—N str.), 1230(C—O str.), 1336(C—O str.), 1436, 1468(C—H bend.), 1603(C═C str.), 1657(C═N str.), 2854(>CH_2 str.), 2935(>CH_2 str.), 3010(=C—H str.), 3061(=C—H str.). UV–*Vis* (DMSO, 1 $\times 10^{-5}$ M): λ_{max}(nm), (logε): 322 (4.99), 635 (4.45), 709 (4.99). MS *(*MALDI-TOF*) m/z* : calc.: 1176.98; found: 1177.93 $[M+H]^+$.

2.2.3. 1(4),8(11),15(18),22(25)-Tetrakis-(2,6-dimethoxyphenox) phthalocyaninato manganese(III)acetate (5)

The MnPc (**5**) is soluble in toluene, $CHCl_3$, DCM, THF, DMF and DMSO. Mp > 300° C. Yield: 8.79 mg (27.7%). Calculated for $C_{66}H_{51}MnN_8O_{14}$: C, 64.18%; H, 4.16%; N, 9.07%; found C, 64.33%; H, 4.27%; N, 9.17%. FTIR (ATR) λ_{max}/cm^{-1}: 879, 970, 1077(C—C str.), 1108(C—N str.), 1252(C—O str.), 1323(C—O str.), 1472(C—H bend.), 1601(C═C str.), 1663(C═N str.), 1707(C═O str.), 2871(>CH_2 str.), 2945(>CH_2 str.), 3016(=C—H str.), 3071(=C—H str.). UV-*Vis* (DMSO, 1 $\times 10^{-5}$ M): λ_{max}(nm), (log ε): 334 (4.75), 364 (4.74), 517 (4.09), 715 (4.62), 764 (5.09). MS *(*MALDI-TOF*) m/z* : calc.: 1176.07; found: 1177.21 $[M\text{-}OAc+H]^+$.

2.2.4. 1(4),8(11),15(18),22(25)-Tetrakis-(2,6-dimethoxyphenoxy) phthalocyaninato nickel(II) (6)

The NiPc (**6**) is soluble in toluene, $CHCl_3$, DCM, THF, DMF and DMSO. Mp > 300° C. Yield: 10.70 mg (33.6%). Calculated for $C_{64}H_{48}N_8NiO_{12}$: C, 65.15%; H, 4.10%; N, 9.50%; found C, 65.00%; H,

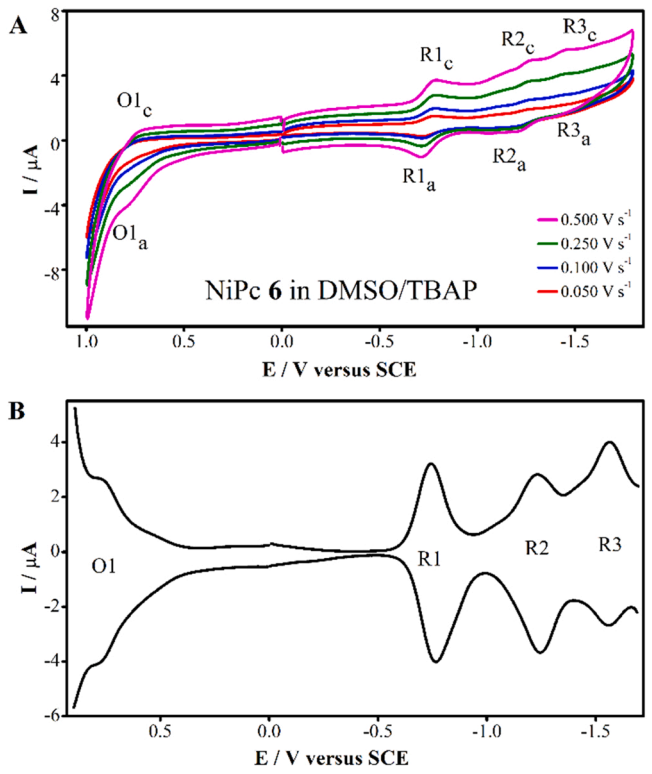

Fig. 3. Cyclic and square wave voltammograms of NiPc **6** on Pt in TBAP/DMSO.

4.25%; N, 9.66%. FTIR (ATR) λ_{max}/cm^{-1}: 887, 936, 974(C—C str.), 1025, 1088(C—C str.), 1136(C—N str.), 1158(C—N str.), 1245(C—O str.), 1316, 1345(C—O str.), 1442(C—H bend.), 1461(C—H bend.), 1598 (C═C str.), 1672(C═N str.), 2859(>CH_2 str.), 2945(>CH_2 str.), 3017 (=C—H str.), 3059(=C—H str.). UV–*Vis* (DMSO, 1 ×10^{-5} M): λ_{max}(nm), (log ε): 346 (4.36), 630 (4.09), 671 (4.25), 701 (5.08). MS *(*MALDI-TOF*) m/z* : calc.: 1179.01; found: 1179.02 $[M]^+$.

2.3. Electrochemical, in situ spectroelectrochemical and electrocatalytic measurements

A Gamry Reference 600 potentiostat/galvanostat was utilized for cyclic voltammetry (CV) and square wave voltammetry (SWV) measurements. In these voltammetric measurements, the analyte, i.e., the solution of a Pc in ultra-pure DMSO involving electrochemical grade tetrabutylammoniumperchlorate (TBAP) as the aiding electrolyte at a concentration of 0.10 mol dm^{-3} was placed in a cell with reference, counter and working electrodes configuration at 25 °C. A Pt plate and a Pt spiral wire were used as the working and counter electrodes, respectively, while a saturated calomel electrode (SCE) was used as the reference electrode. The analyte solution was deoxygenated for fifteen minutes prior to each run by high purity of N_2. For controlled-potential coulometer (CPC) measurements were operated with transparent Pt gauze having a surface area 10.5 cm^2 as a working electrode, a Pt wire as a counter electrode and a SCE as a reference. An Ocean Optics HR2000 UV–*Vis* spectrophotometer was combined with the Gamry Reference 600 potentiostat/galvanostat for *in situ* spectroelectrochemical and *in situ* electrocolorimetric measurements. An optically transparent thin layer (OTTLE) cell with three-electrode configuration at 25 °C was utilized for the measurements. Electrocatalytic rotating disk electrode (RDE) measurements for MPc-catalyzed oxygen reduction reaction (ORR) have been performed with the Gamry Reference 600 potentiostat using a glassy carbon disk as the working and a wire as the counter electrodes, and a SCE as the reference. A glassy carbon disk with 5 mm dia in O_2 saturated 0.50 M H_2SO_4 aqueous solution under quasi-stationary conditions (0.005 Vs^{-1} sweep rate) at 25 °C Rotating ring-disk electrode (RRDE) measurements were performed by combining two Gamry Reference 600 potentiostats. A platinum ring leading to a collection efficiency, N = 37%, the working electrode was a glassy carbon disk (5.61 mm dia). These analyses were achieved at 2500 rpm in the system absence of oxygen 0.5 M H_2SO_4 aqueous electrolyte solution at 25∘C. The disk potential was scaned at 0.005 V s^{-1} whereas the ring potential was carried on 0.95 V vs. SCE. A Pine Instrument Company AFMSRCE modulator speed rotator was run for dynamic RRDE and RDE voltammetry analyses. 5% Nf solution (Aldrich), Vulcan XC-72 (VC) (Cabot Co.), extra-pure ethyl alcohol (Merck), and Pcs were utilized in catalyst arrangement. Platinum ring-glassy carbon disk electrode, glassy carbon disk electrode and a burnishing kit were shopped from Pine Instruments. So as to order to diffuse the catalysts on a glassy carbon disk electrode for RRDE analysis, a concoction of 0.8 mg Pc, 1.2 mg Vulcan and 10 µL 5% wt Nafion solution in 200 µL absolutist ethanol was arranged and homogenized via ultrasonic way for 30 min. The required amount of this ink was covered via a micropipette onto a newly burnished GCE by loading catalyst of 106 µg cm^{-2}. The presence adjusted volume of Nf in the catalyst ink was been chosen so as to make the catalyst film adequately thin, because of that diffusion resistance of the film was inconsequential.

With the purpose of covering the GCE totally, after settling the ink drying process was applied quickly. Voltammograms were obtained with fresh preparations on the electrode surface. A SCE electrode was used as reference electrode and a Platin spiral wire was used as a counter electrode.

3. Results and discussion

3.1. Synthesis and characterization

The starting material **1** and compound **2** were synthesized according to the literature [26]. Unfortunately, the yield was remarkably low when compound **2** was synthesized using the procedure reported in the same literature. Therefore, a different synthetic pathway with two steps was used to prepare **2** at relatively higher yield (41%)(Scheme 1) [27]. Firstly, the dilithium Pc achieved by using 3-(2,6-dimethoxyphenoxy)−1,2-dicyanobenzene (**1**) in n-pentanol [28]. Dilithium Pc is unstable against various acids and water. It is easy to turn into the metal free phthalocyanine [29]. In the second step, dilithium Pc was converted to compound **2** by adding acetic acid.

Conversion of the H_2Pc (**2**) into the MPcs (**3-6**) was achieved by refluxing this compound in n-pentanol in the existence of the relevant metal salts [$Co(OAc)_2$.4 H_2O, $Fe(OAc)_2$, $Mn(OAc)_2$.4 H_2O or $NiCl_2$] and DBU under N_2 atmosphere for 2 h. Under these reaction conditions Mn (II)Pc transformed Mn(III)Pc. While tetrapyrrole derivatives such as Fe (II) and Mn(II)porphyrin and Fe(II)Pc and Mn(II)Pc are synthesized and purified, they usually transform into Fe(III) and Mn(III) porphyrin and Fe(III)Pc and Mn(III)Pc or their mu-oxo-dimers because of the aerobic conditions [30,31].

All MPcs (**3-6**) were purified by two-steps column chromatography separation technique, using the appropriate solvent systems of $CHCl_3$: MeOH (9:1) and solely THF, respectively. The yields for the MPcs **3**, **4**, **5** and **6** were 30.2%, 23.5%, 27.7% and 33.6%, respectively. These reaction yields are quite low compared to their beta-substituted analogues MPcs[23]. This result can be explained by the fact that the electron-releasing dimethoxy groups, which are distant substituents, donate more electrons to the ring via the alpha oxo-bridge and the partial positive charges of the nitrile carbons decrease. Since the Pc synthesis mechanism starts with the attack of the nucleophiles on the nitrile carbons, the reaction rate and the reaction yield decreases[32].

The elemental investigation, UV–*Vis*, FTIR and the MALDI-TOF mass spectroscopic output affirmed the planned formations of these novel Pcs.

The FTIR spectra of the H_2Pc (**2**) and MPcs (**3-6**) were quite similar,

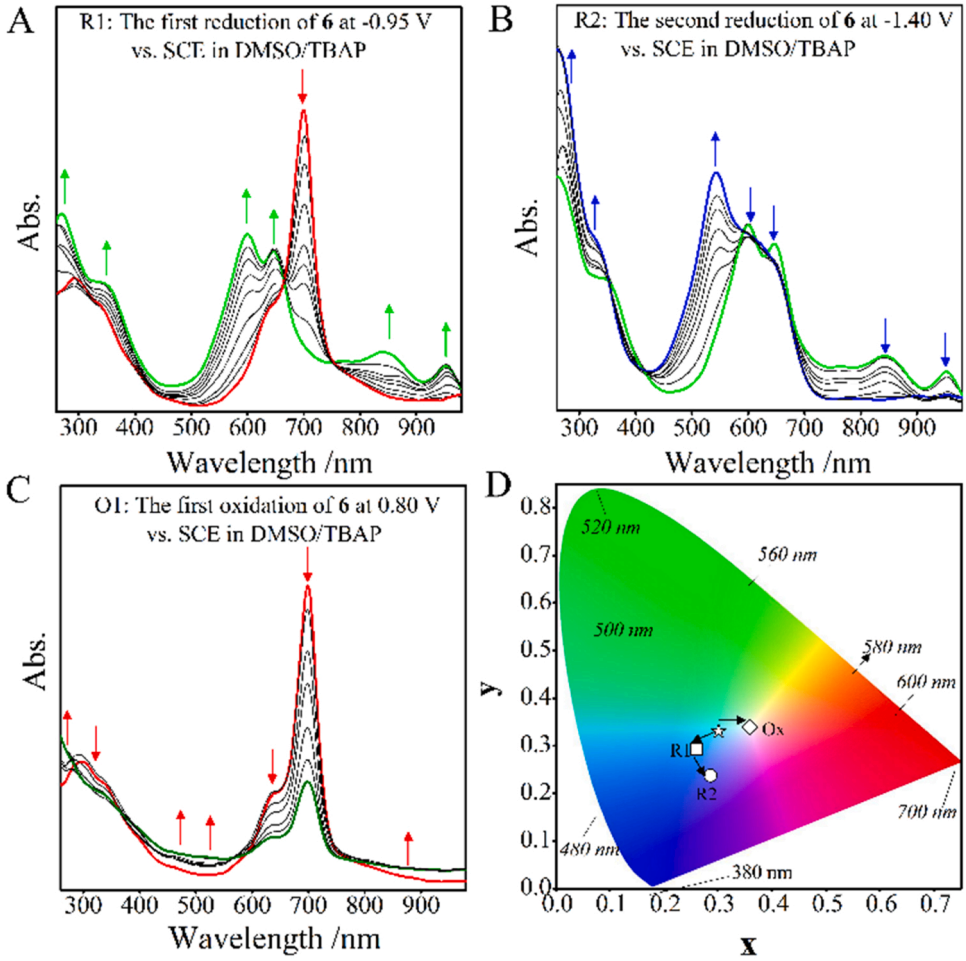

Fig. 4. *In situ* UV-*Vis* spectral changes recorded for the electrochemical redox processes of NiPc 6 (A-C) and the coupled colour changes (D) on Pt in TBAP/DMSO.

apart from the -NH stretching oscillation of the central core in metal free Pcs. The –NH groups of the H_2Pc (**2**) in the central core provided feeble absorption peak at 3286 cm^{-1}. The pointed peak for the −C≡N vibration of band at 2231 cm^{-1} for the compound **1** disappeared after Pc formation in the FTIR spectrum. In the FTIR spectrum for the MPcs (**3-6**), vibrations bands were detected at 3010–3071 cm− 1 for aromatic C–H stretching, 2854–2945 cm^{-1} for aliphatic C–H stretching, 1598–1605 cm^{-1} for aromatic C=C stretching and 1230–1253 cm^{-1} for Ar–O–Ar stretching (Fig. S1).

The electronic absorption behaviour of **3-6** was explored via UV-*Vis* spectroscopy in disparate solvent systems such as DMSO, DMF, THF, DCM, toluene and chloroform (Fig. 1). The UV-*Vis* spectrum of DMSO solutions (at 1.00×10^{-5} M) of the non-peripherally 2,6-dimethoxyphenoxy substituted cobalt(II), iron(II), manganese (III) and nickel(II) Pcs (**3**–**6**) displayed distinctive absorption which via Q bands at 692, 709, 764 and 701 nm, respectively. The B bands for the MPcs observed at 319 nm for **3**, at 322 for **4**, at 364 nm and 334 nm for **5** and at 346 nm for **6** (Fig. 1). When the Q bands of alpha-substituted Pcs are compared with their beta-substituted analogues [23], red shifting occurred at 27 nm for CoPcs, 36 nm for Mn(OAc)Pcs and 33 nm for NiPcs in accordance with the literature [33]. Although iron phthalocyanines are synthesized as Fe(OAc)Pc in beta substituted analogues, they were synthesized as FePc in this study.

The Q band observed for the Pc complexes was attributed to the π-π * transition from the highest occupied molecular orbital (HOMO) to the lowest unoccupied molecular orbital (LUMO) of the Pc ring. The other bands (B) in the UV region at 315–375 nm were observed due to the transitions from the deeper p levels to the LUMO [34]. It is known that Pc aggregation causes decline on the magnitude of the Q band belongs to the monomeric species; in addition, it can also been observed that the absorbance of a novel expansive blue shifted band rose. When the UV-*Vis* spectra of the MPcs are examined carefully, a slight shoulder peak between the Q band and the vibration band in all solutions of the NiPc **6** was observed. This suggests that the solutions contain trace amounts of H aggregated species. The spectrum of CoPc **3** had a lone narrow and non-splited Q band in most of the solvents except DMSO. But the vibration band of the spectrum of CoPc **3** in DMSO became broad because of trace amounts of H aggregated species like the UV-*Vis* spectrum of NiPc **6**.

In addition, the Q band of MnPc was observed at 760 nm, indicating that the Mn ion in the center of this Pc is + 3 valences. Mn(II)Pc, Mn(II)Pc(X)$_2$ (X coordinating solvent), (Mn(III)Pc)$_2$O, or Mn(III)Pc kinds may observe during the synthesis, purification and electronic spectra measurements of MnPcs. The occurrences of these species also depend on the molecular structure of the Pc complexes. It generally can be predicted the existence of these species by looking to the values of Q band in UV-*Vis* spectrum. Usually, peaks in the spectrum in the range of 700–750 nm, 660–700 nm and 600–645 nm, indicate the presence of Mn(III)Pc, Mn(II)Pc and Mn(II)Pc(X)$_2$ (X: coordinating solvent) or Mn(III)Pc)$_2$O, respectively [35]. In addition, when any solution of MnPcs are kept in the open air, species can transform into each other depending on solvent [35]. Similar interpretations can be made for FePcs[30]. When Fig. 1C is carefully examined, Mn(III)Pc species is dominant in DMSO solution and Mn(II)Pc species is dominant in toluene solutions. However, in the remaining solvents (DMF, THF, chloroform and dichloromethane) Mn(II)Pc and Mn(III)Pc are observed as a mixture. In

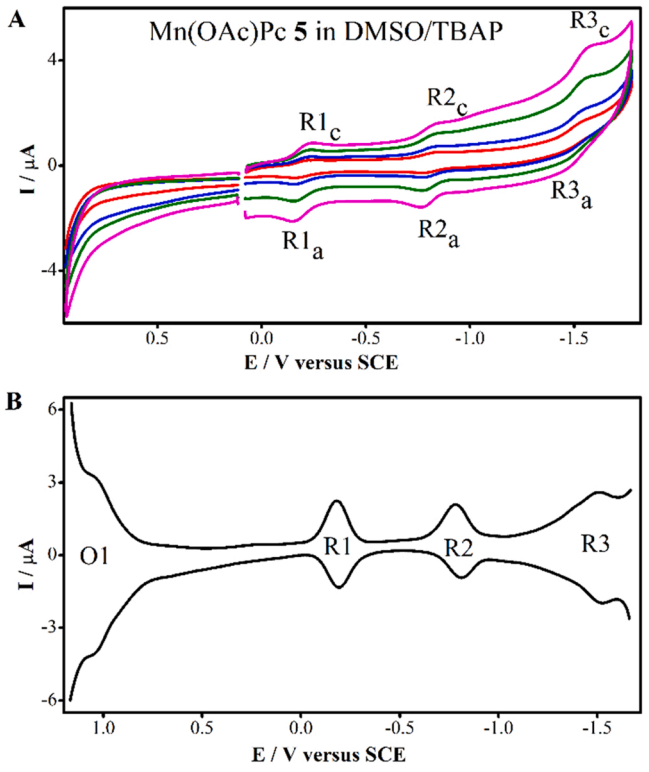

Fig. 5. Cyclic and square wave voltammograms of Mn(OAc)Pc **5** on Pt in TBAP/DMSO.

addition, DMF solution contains trace amounts of $Mn(III)Pc)_2O$ kinds.

When the UV-*Vis* spectrum of Fe(II)Pc were examined, red shifted shoulder peaks were found to the right of the Q band in chloroform, dichloromethane and THF because of slightly Fe(III)Pc species and blue shifted shoulder peak were found to the left of the Q band because of slightly mu-oxo-dimer species in DMSO (Fig. 1).

This paper has investigated the aggregation behaviours of Pcs (**3–6**) at varying concentrations in DMSO. All of these MPcs were appropriate for the Beer-Lambert law with the changing concentration between 1.20×10^{-5} M and 2.10^{-6} M (Fig. 2). While CoPc **3**, Fe(II)Pc **4** and NiPc **6** showed low degree of aggregation at this concentration range, Mn(III) Pc **5** did not show any aggregated species (Fig. 1 and Fig. 2).

The molecular structure of all the novel Pcs (**3-6**) have been identified by MALDI-TOF mass spectrometry using dihydroxybenzoic acid (DHB) as matrix of MALDI in the mode of reflectron. Mass spectra of **3–6** are shown in Fig. S1. While ionic peak belonging to the molecule $[M]^+$ of nickel(II) Pc (**6**) was observed at *m/z*: 1179.02 Da, the $[M+H]^+$ peaks of the cobalt (II) Pc(**3**) and the iron (II)Pc(**4**) were recorded at *m/z*: 1181.13 and 1177.93, respectively. The $[M+H\text{-}OAc]^+$ peak of manganese(III) Pc(**5**) were observed at and 1177.21 Da. Moreover, the H_2O adducted molecular ion peak $[M+H_2O]^+$ of cobalt(II) Pc (**3**) were also recorded at *m/z*: 1198.13 Da (Fig. S2).

3.2. Electrochemistry, in situ spectroelectrochemistry and electrocatalysis for ORR

MPcs display metal and/or ligand-based electron transfer redox processes, which have different characteristics depending on the different agents for instance solvent polarity, sort of substitution, the nature of the centered metal and some aggregational effects. Complete identification of the redox behaviour of newly synthesized Pcs is crucial in terms of understanding their applicability in various fields of electrochemical technologies such as electrocatalysis and electrochromism. The electrochemical properties of MPcs **3-6** were identified via cyclic voltammetry and square-wave voltammetry in DMSO including TBAP that is the auxiliary salt. Furthermore, *in situ* spectroelectrochemical analyses provided supplementary backing for complete description of the electrochemical processes, which are either metal or ligand based. Table 1 lists the electrochemical output of the redox processes of the \MPc complexes and compared with recently reported electrochemical data of the corresponding beta-tetra substituted Pcs [23]. In general, MPcs displayed consecutive one-electron quasi-reversible or reversible electron transfer processes with the anodic to cathodic peak separations, ΔE_p values inside the interval of 80–120 mV. Usually, currents of the peak are straight commensurate to the square-root of the scan rate [36], indicating the move of electroactive species via diffusion controlled to the working electrode (Fig. S3). In Table 1, redox potentials of **3-6** have been examined in contrast to their formerly announced unsubstituted [14,37,38] and tetra-substituted [30,39,40] analogues. The redox processes having half peak potentials of the **3-6**, were shifted negatively according to others. The electron releasing effect can caused this potential shifting of four dimethoxyphenoxy groups at non-peripheral positions of **3-6** [24]. On the other hand, the voltametric responses of **3–6** seem incorporating electron-releasing substituents to non-peripheral sharper and more reversible, compared to some similar MPc complexes, previously reported by our group [30,39,40]. It is clear that positions of MPc complexes does not only increase their solubility but also enhances the quality of their redox signals.

Cyclic voltammograms (CVs) and square wave voltammograms (SWVs) of NiPc **6** can be seen in the Fig. 3. This Figure shows an oxidation and three reductions couple, which are usually reversible as confirmed by ΔE_p values and the current ratios of the peak. In order to describe which redox process belongs to the Pc ring or metal center, it should be focussed on the changes in the UV-*Vis* spectrum with these processes while applying the electrochemically the constant potential for each redox process in DMSO/TBAP electrolyte system (Fig. 4). During the application of an advisable consistent voltage for both first and second reductions in Fig. 4A and Fig. 4B respectively, and the first oxidation in Fig. 4C, the magnitude of the Q-band absorption declines without shifting and a novel absorbance band appears in the scale of 500–600 nm. These spectral changes are distinctive for redox processes that belonging to Pc ring-based in MPcs and clearly suggest that **6** has all ligand based redox processes [41]. Furthermore, in the initial spectrum having the 650 nm band before the controlled-potential electrolysis at a suitable constant potential should coincide to the species being aggregated. In the area of 550–650 nm two new bands that were formed while the electrochemical first redox process at − 0.65 V provide further backing for the existence of aggregation in the medium since the aggregated species of Pcs is usually mirrored by expanding or splitting of the Q-band absorption [14] (Fig. 4A). In the deficiency of aggregation, the formation of a novel wave in the area of 500–600 nm is expected when a ring-based reduction occurs. Nonetheless, upon the first reduction, two new waves and thus, at 600 nm a split Q-band form the band probably correlates to the aggregation while the other one at 650 nm is belong to monomeric reduced species since aggregation is usually causes shifting to blue. In the area of 842 and 950 nm novel bands composed while the first reduction process also points out its ligand-based character. During the second reduction process at constant − 1.40 V, the band for aggregated species at 600 nm shifts 540 nm with a rise in intensity and the absorbance of the band correlating to monomeric kinds declines while bands declines at 842 nm and 950 nm without any shifting (Fig. 4B). All spectral differences for **6** are characteristic for reduction processes of ligands despite some deviations resulting from the aggregation. The changes in the absorbance spectrum observed in the course of the first process at 0.80 V are distinctive for a Pc ring-based electron transfer process (Fig. 4C). Upon the electrolysis at constant potential, at 700 nm the main Q band declines without shift and a novel band forms in the area of 500 nm and 600 nm. Without any potential application, the neutral form of $[Ni^{II}Pc^{2-}]$ complex had a light blue colour. After applying − 0.95 V constant potential, colour of initially **6**

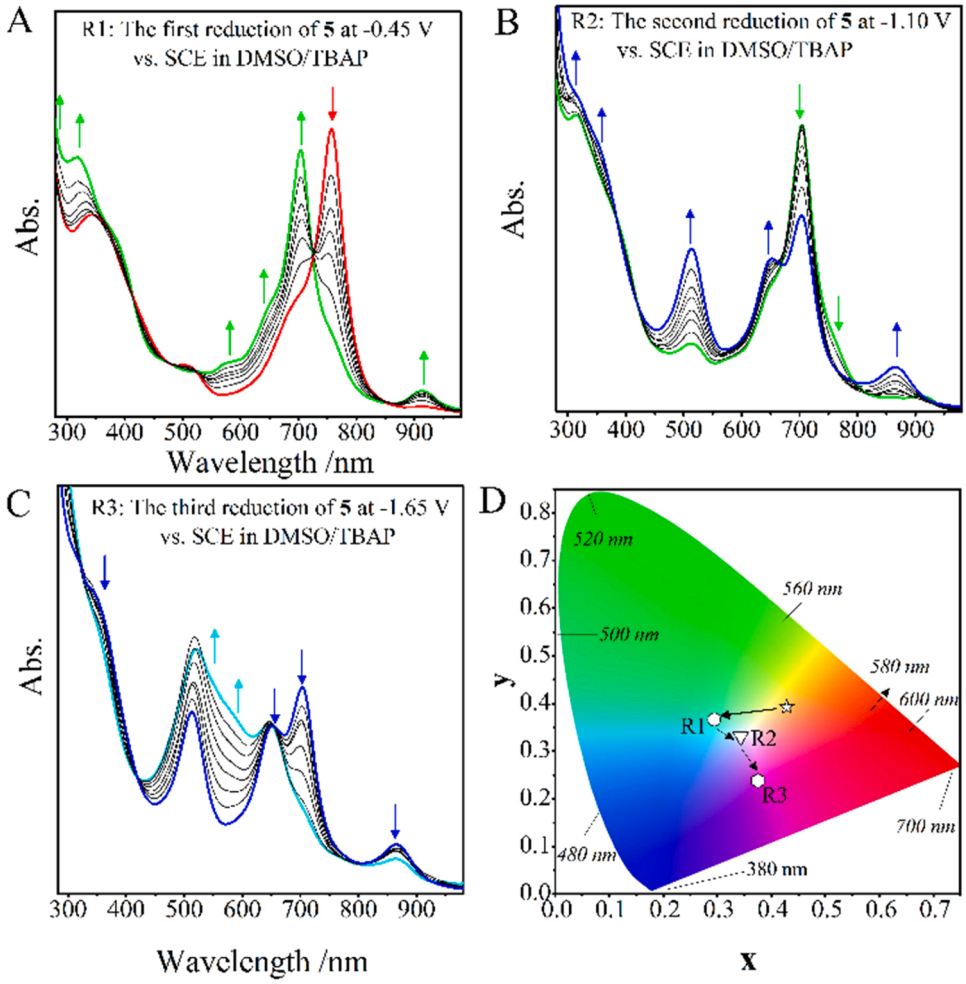

Fig. 6. *In situ* UV-*Vis* spectral changes recorded for the electrochemical redox processes of Mn(OAc)Pc 5 (A-C) and the coupled colour changes (D) on Pt in TBAP/DMSO.

changed into blue at the point of finishing the first redox reduction. Afterwards the first reduction process, − 1.40 V constant potential was implemented for second reduction processes, and the light purple colour was acquired (Fig. 4D). The oxidation processes also lead to the transformation of the original light blue colour the solution of NiPc **6** into light yellow colour. The association of a net colour change with the redox processes suggests that NiPc **6** is suitable for testing for electrochromic devices (Fig. 4D). The electrochemical redox behaviour of the other complexes CoPc **3**, FePc **4** and MnPc **5** has been observed to be highly different from that of the NiPc **6**. It can be understood from the Table 1 that the first oxidation and reduction processes of these MPc complexes occur much easily with respect to those of NiPc **6**. Thus, the distinction between the first reduction and first oxidation half-peak potentials of these MPcs is really small as compared to **6**, probably due to their metal-based filled or semi-filled d orbital energy levels, which are located on the energies of the highest occupied transfer process, i.e., the first oxidation and the first reduction. Additionally, it appears that NiPc complex **6** does not have this type of d orbital energy levels betwixt the LUMO and HOMO. Therefore, center of NiPc **6** have redox inactive metal behaviour because of Ni(II) metal. Thus, all processes for this type of MPcs are ring (ligand) based redox reduction and oxidation processes. If the central metal behaves as a redox-actively and the first electron transfer process, i.e., the first oxidation and the first reduction occurs on the redox active metal centered in the Pc ring. On the contrary, it appears that complex NiPc **6** does not have this type of d orbital energy levels betwixt the LUMO and HOMO. Furthermore, distinction between the first reduction and the first oxidation processes coincides to the LUMO-HOMO gap with the limits of 1.50–1.80 V.

for the MPcs (Table 1). On the other hand, this potential difference for the MPcs having active metal center in redox processes for instance MnPc, FePc and CoPc does not coincide to the HOMO-LUMO gap of the Pc ligand. Fig. 5 shows cyclic and square wave couple, which could be monitored only with SWV. Probably, voltammograms of Mn(OAc)Pc **5** in DMSO. It displays three reversible one-electron reductions and a reversible oxidation Mn^{II}/Mn^{I} couples while the last one is observed due to the Pc^{2-}/Pc^{3-} process. On the other hand, the oxidation couple should result from Pc^{2-}/Pc^{-} process as confirmed by its considerably positive peak potential. The changes in the absorbance spectrum in UV-*Vis* monitored while the potential controlled electrolysis of Mn(OAc)Pc **5** at constant voltages are shown in Fig. 6. The absorption at 758 nm is a strong Q-band, which suggests that manganese metal center has the oxidation state of three (Fig. 6A). Under the − 0.45 V constant potential the original Q band disappears and shifts 704 nm as a new strong band for the first reduction redox process. Meanwhile a novel small band appears at 915 nm and the B band was shifted from 343 nm to 317 nm. The band that is at 758 nm shifted to 704 nm as the novel band appeared, this spectral change is strongly confirm that Mn(OAc)Pc **5** has a metal based process as the first reduction process Mn^{III}/Mn^{II}. The changes in the absorbance spectrum are correlated with the change of colour from original reddish brown to green as shown in Fig. 6D. Under the constant − 1.10 V associated with second reduction, the peak at 915 nm continues to increase and the band at 704 nm declines while a

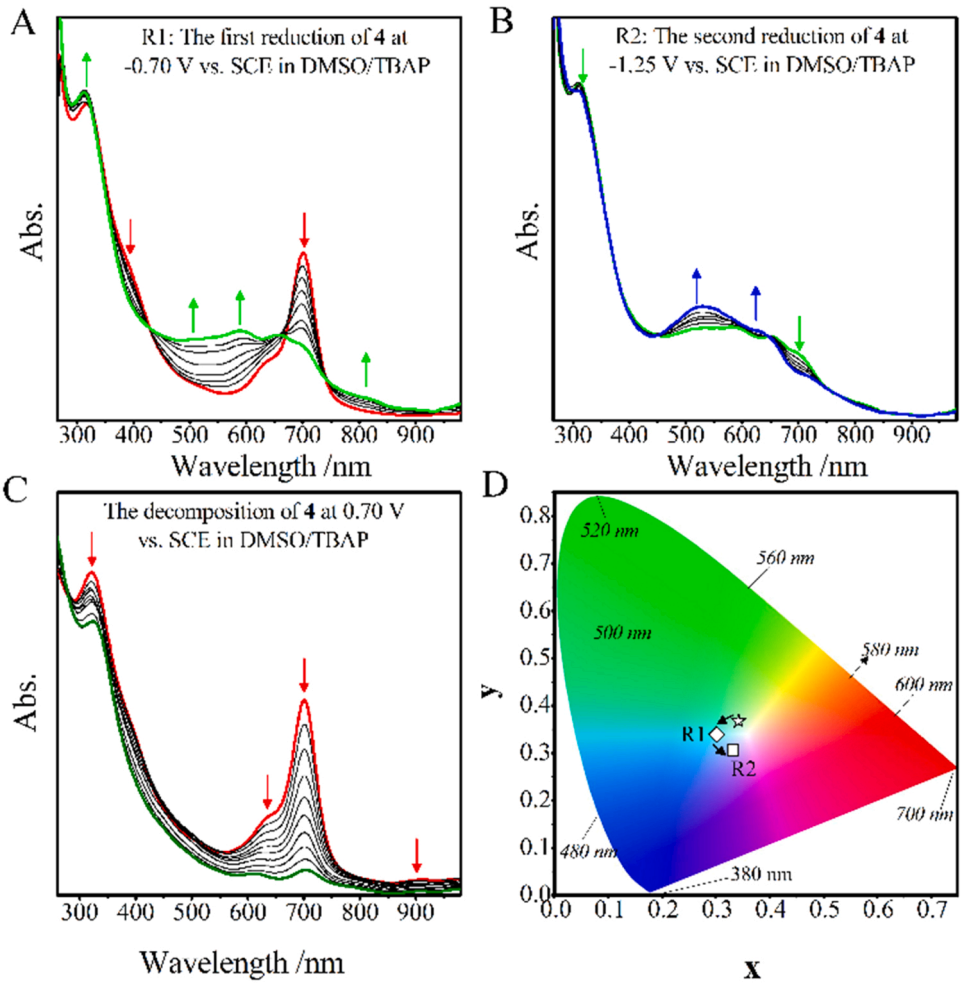

Fig. 7. *In situ* UV-*Vis* spectral changes recorded for the electrochemical redox processes of FePc 4 (A-C) and the coupled colour changes (D) on Pt in TBAP/DMSO.

strong band at 515 nm forms (Fig. 6B). In the second reduction process, the novel band at 515 nm points out that it is a metal based redox process (Mn^{II}/Mn^{I}). Fig. 6D shows that the changing in the colour from green to blue is indicated by *in situ* electrocolorimetric measurements. Applying the constant − 1.65 V vs. SCE is associated with the third reduction process that causes a new band between additional 500 and 600 nm and decreasing at the 704 nm with no shifting (Fig. 6C). In the changes of absorbance spectrum for that process are distinctive for Pc ring-based electron transfer process (Pc^{2-}/Pc^{3-}), which gave rise to shift in the colour from blue to turquoise.

The distinct multi changes in the colour correlated with the reduction redox processes of Mn(OAc)Pc **5** shows that it is a good material for testing in electrochromic devices. As shown in Table 1 and Fig. S4 in the Sup. Info., FePc **4** shows a one- electron oxidation and three one-electron reductions, probably as the redox couples Fe^{II}/Fe^{I} (R1), Pc^{2-}/Pc^{3-} (R2), Pc^{3-}/Pc^{4-} (R3), and Fe^{II}/Fe^{III} (O1), respectively. The assignment of these redox processes to metal or Pc ligand has also been confirmed by the combination of electrochemical and UV-*Vis* spectral measurements, i.e., *in situ* spectro-electrochemistry. Fig. 7 shows spectral and colouring changes recorded through the R1, R2 and decomposition processes of FePc **4**. Under the constant − 0.70 V vs. SCE associated with first reduction process, sharp band at 700 nm declines in intensity and broadens. That band also shifted to 680 nm that is accompanied by the creation of a new broad band between 435 and 635 nm (Fig. 7A). In the changes of absorbance spectrum, especially the blue shifting of the main Q band is characteristic and unique for the metal-based reduction processes, during R1 Reduction process (Fe^{II}/Fe^{I}). In the R2 reduction process under the − 1.25 V resulted decrease in the absorption band at 680 nm and the broad band between 435 and 635 nm continued to increase, implying that it is a Pc ring-based Pc^{2-}/Pc^{3-} process (Fig. 7B).

During the R2 process the original green colour turned into the blue as shown in Fig. 7D. As shown in Fig. 7C, all absorption bands of FePc **4** decreases under the constant + 0.70 V. It appears that controlled-potential process at a considerably high positive potential, complex **4** decomposes immediately after the O1 process. Furthermore, changes in the colour of the solution of FePc 4 in DMSO at + 0.70 V applied potential was followed by *in situ* electrocolorimetric measurements as monitoring of the colour index. Two reductions and two oxidations processes are observed in the square-wave and cyclic voltammograms of CoPc **3** (Fig. 8). From the well-known redox behaviour of cobalt Pc compounds in polar solvents, these redox processes can be assigned as R1 at − 0.40 V $[Co^{II}Pc^{2-}]/[Co^{I}Pc^{2-}]^{-}$, R2 at − 1.41 V $[Co^{I}Pc^{2-}]^{-}/[Co^{I}Pc^{3-}]^{2-}$, O1' at 0.36 V $[Co^{II}Pc^{2-}]/[Co^{III}Pc^{2-}]^{+}$ and O1'' at 0.51 V, and O2 at 0.86 V $[Co^{III}Pc^{2-}]^{+}/[Co^{III}Pc^{-}]^{2+}$. The splitting of the O1 wave may be assigned to the existence of aggregation, especially at the positive applied potentials. The association of the aggregation phenomenon with the redox processes of Pc complexes is a well-known situation in the literature [42].

Voltammetric data suggests that the electron transfer processes of CoPc **3** are reversible at low scan rates and becomes quasi-reversible at relatively high scan rates, with the anodic to cathodic peak separation values in the interval of 0.060–0.120 V.

Spectroelectrochemical measurements at suitable constant peak potentials supported evidence for the electrochemically assigned redox

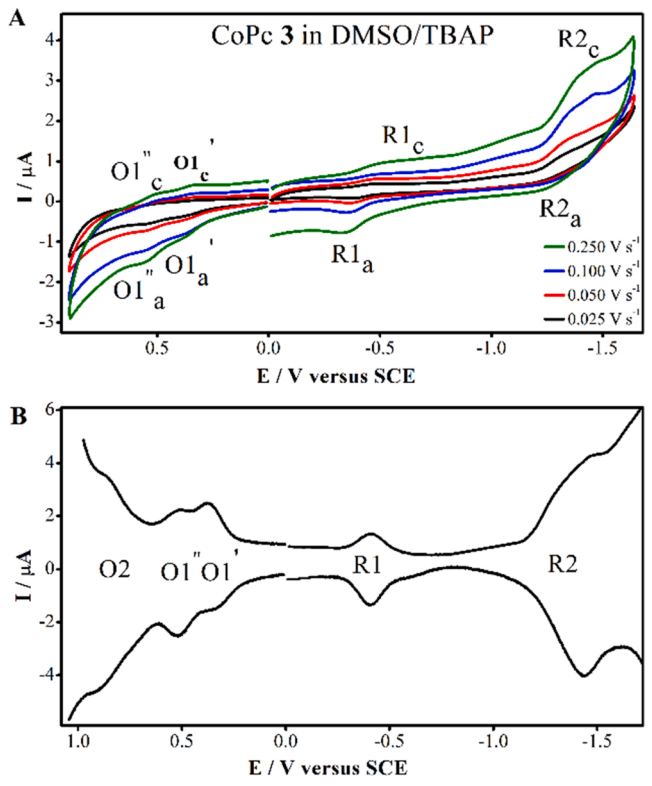

Fig. 8. Cyclic and square wave voltammograms of CoPc 3 on Pt in TBAP/DMSO.

processes of CoPc **3** and the presence of aggregated species (Fig. 9). The broad peak at 620 nm in the absorbance spectrum of CoPc **3** before applying any potential can be regarded as an indicator for the presence of aggregation. For the R1 process at − 0.65 V vs. SCE, this broad shoulder nearly disappears, the main band shifted from 687 to 715 nm and a novel band formed at 460 nm (Fig. 9A). The formation of a novel band in the interval of 400–500 nm and the shifted Q-band are is unique for metal-based reduction processes of MPc complexes and thus, support Co(II)/Co(I) assignment for the R1 process of CoPc **3** [43]. Under the constant − 1.60 V potential for R2 process the intensity of the Q band declines without shift and a novel band appears at 564 nm (Fig. 9B). The changes in the absorbance spectrum confirm that the second reduction process of CoPc **3** is a Pc based redox process since decreasing of the Q-band with no shifting and the creation of a novel band in the range of 500 and 600 nm are distinctive spectral changes for the Pc ring-based redox processes [44]. The spectral changes in Fig. 9C are observed under the constant + 0.65 V for the O1 of CoPc **3** at vs. SCE. Upon this electrolytic process, the Q band intensity declined and shifted from 700 nm to 687 nm. These changes in the absorbance spectrum are unique for metal-based oxidation process. Thus, these spectral changes approves the O1 process as $[Co^{II}Pc^{2-}]/[Co^{III}Pc^{2-}]^{+}$ couple [45]. While the original turquoise colour of the solution turned into blue colour after applying + 0.65 V potential, in the course of the first and second reduction processes, the original colour of the solution of CoPc **3** in DMSO changed to blue and red, respectively (Fig. 9D). The association of distinct and colour changes to the redox processes of CoPc **3** in the solution implies that it is an excellent aspirant for electrochromic devices.

The comparison of the $\Delta E_{1/2}$ values of **3-5** with those of **6** also strongly suggests that the MPc complexes involving a redox active metal in the ring centre can be easily oxidized and reduced in comparison with complexes containing a redox inactive metal centre (Table 1). Redox conducts of metal in the ring centre causes redox differences because of the d-orbital energy levels of metals taking position betwixt the LUMO and HOMO energy levels of the Pc ligand. Then, because of the central redox active metal, the Pc ring is reduced or oxidized after the metal in the ring centre during the potential scan towards the negative or positive values, respectively. In this study, this comment was also confirmed by the analysis of *in situ* spectral changes monitored while applying suitable constant reduction or oxidation potentials to the system that includes complexes. Pc complexes with central redox-active metal usually display high catalytic activity, especially for oxygen-, hydrogen- and water-based reduction and oxidation processes [46]. The electrocatalysis of these processes has vital importance for various energy converting and storing systems, for instance different types of fuel cells [47–51].

In this study, electrocatalytic performances of the MPc compounds have also been tested by RDE technique at 2500 rpm electrode rotation and 0.005 Vs^{-1} potential sweep rates, recording linear sweep voltammograms (LSVs) with MPc modified electrodes including VC as the supporting carbon-based material and Nf as the binder in O_2-saturated aqueous acidic medium (0.50 M H_2SO_4) (Fig. 10A) [52].

For each MPc catalyst, electrocatalytic performances were appraised by considering the limiting diffusion current density (J_L) and the onset potential (E_o) that is at the point the current density being 0.100 mA cm^{-2}. Table 2 presents the electrocatalytic performance of MPc-based catalysts for oxygen reduction reaction. As clearly shown in this table, J_L values of **3-5**, especially CoPc **3**, are much higher than that of NiPc **6**. The J_L takes the value of 3.08 mA cm^{-2}. The comparison of this value with those in the literature implies that ORR reaction on the VC/Nf/CoPc modified GCE involves a mechanism going to completion through a two steps mechanism containing two electrons transfer in each step to produce first hydrogen peroxide and then, water and/or a direct one-step 4 electrons mechanism to give water [53]. Additionally, E_o value for **6** is more negative than values of **3-5**. Especially, E_o value of FePc **4** is much more positive than that of the other complexes. Catalytic performances of **3-5** towards ORR are much better as compared to that of **6**. The electrocatalytic data implies that redox-active metal centre has a remarkable positive influence on the OR kinetics. Another reason for good catalytic activity for ORR is also the good solubility of the complexes due to the non-peripheral dimethoxyphenoxy substituents and therefore, their good dispersion in the catalyst ink.

In acidic medium, there are two possibilities for oxygen reduction reaction, two electrons reduction to create hydrogen peroxide leading to low catalytic activity or four electrons transfer to create water corresponding to a desirable situation. In the first case, peroxide can also be turned into water via second two electrons reduction. Thus, identification of the quantity of electrons transferred per dioxygen molecule, n_t makes the evaluation of the addition of the creation of hydrogen peroxide possible. RRDE analyses with a platinum ring electrode polarized at 0.95 V vs. SCE, and a VC/Nf/MPc modified glassy carbon disk electrode were used to measure these contributions of catalysts in the course of ORR. As an example of these measurements, electrocatalytic results of VC/Nf/**4** is presented in Fig. 10B. The quantity of hydrogen peroxide was measured by using the ring currents that initiate at the equal potentials points as like onset potentials and indicate the production of hydrogen peroxide on the disk during ORR. The following equations have been used to determine the n_t and at a given potential the percentage of hydrogen peroxide produced [54–56].

$$n_t = 4 \cdot I_D / [I_D + (I_R / N)] \quad (1)$$

$$\%H_2O_2 = 100 \cdot (4 - n_t)/2 \quad (2)$$

In these equations; N is the collection efficiency, I_D is the disk current and I_R is the ring current. The n_t and $\%H_2O_2$ values for each catalyst at various potentials are shown in Fig. 10C and Fig. 10D. The 4-based electrode produced the best catalytic performance. At all potentials n_t of **4** is higher than **3**, indicating that formation of water is higher to compare with hydrogen peroxide for **4** in ORR. The number of total electrons value rises with augmenting potential and reaches to 3.88 (6% H_2O_2 and 94% H_2O) showing that the main product is water at the

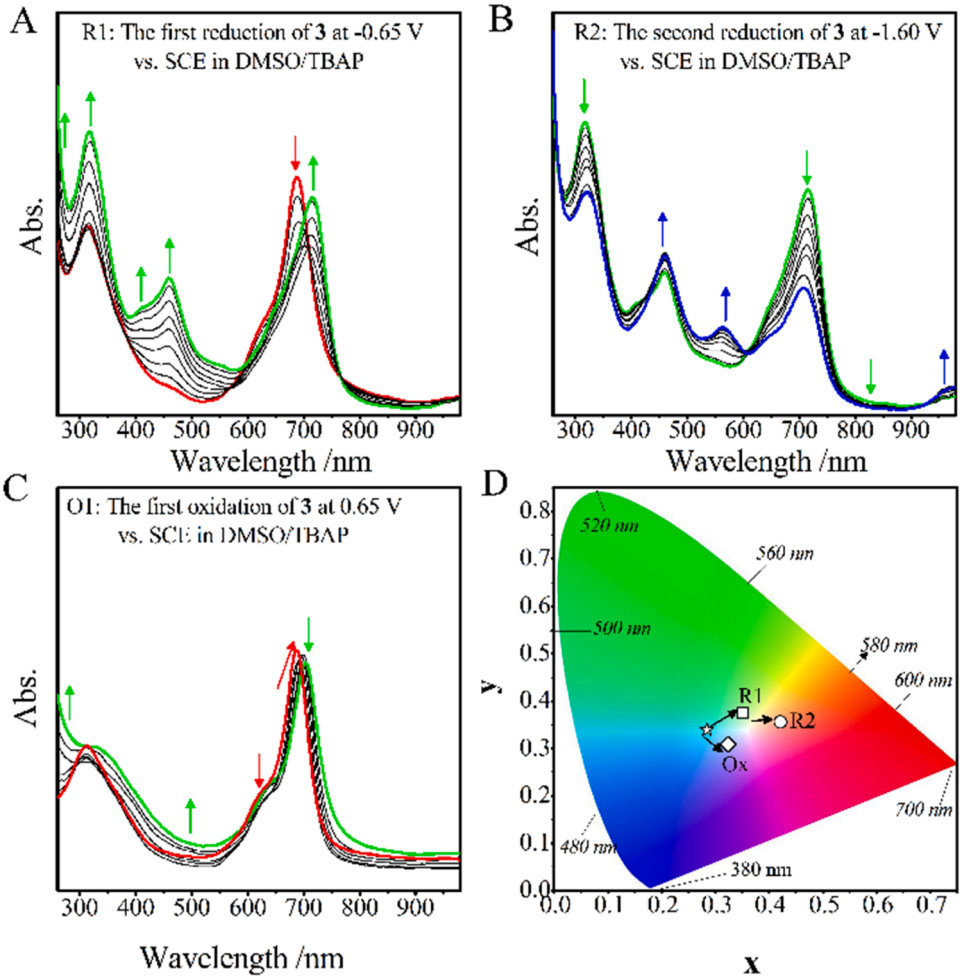

Fig. 9. *In situ* UV-*Vis* spectral changes recorded for the electrochemical redox processes of CoPc 3 (A-C) and the coupled colour changes (D) on Pt in TBAP/DMSO.

limiting diffusion current plane.

4. Conclusions

We have successfully synthesized novel soluble tetrakis non-peripherally substituted cobalt(II), iron(II), manganese(III), nickel(II) phthalocyanines (MPcs **3–6**) and their molecular structures were identified by MALDI-TOF, elemental analysis, UV-*Vis* spectral data, FT-IR, for the first time in this work. The dissociations of novel substituted MPcs (**3–6**) were high in common organic solvents for instance chloroform, dichloromethane, toluene, dimethylsulfoxide, tetrahydrofuran, N, N-dimethylformamide. It could be thought that the non-peripherally 2,6-dimethoxyphenoxy moieties as substituted group and the different metals increased the solubility. Aggregation behaviours of Pc complexes were examined at various concentrations in DMSO/TBAP. The electronic spectra demonstrated a typical monomeric behaviour with a single and tight Q band for phthalocyanine complexes that includes metals and especially the iron at concentration range 1.20×10^{-5} M - 2.00×10^{-6} M. The absorption wavelengths of these MPc complexes extended with the substitution of the 2,6-dimethoxyphenoxy components at on the non-peripheral positions of the Pc skeleton. In the red-shifting behaviour of phthalocyanines, with manganese Pc complex (**5**) showing the largest redshift compared to the others because of the non-planar action of the greater manganese(III) atom that is in the centre. The voltammetric measurements showed that the novel MPc complexes display both Pc- and/or central metal-based electron transfer processes. *In situ* spectroelectrochemical surveys recommended that these Pc complexes- can be considered as the electrochromic materials due to the association of distinct spectral and thus, colour changes to their redox processes. The iron(II) Pc complex **4** had an exceptional catalytic effect for ORR in acidic medium compared to all Pc complexes in this survey because of the rich redox properties of central metal via thanks to breaking ability on the O–O bond. Because the four-electron transfer pathway of **4** is main reaction way, **4** can be considered to have good catalytic results. Well dispersion of this compound in the catalyst ink due to its high solubility was also evaluated to be an additional factor for remarkably good performance for electrocatalytic ORR.

We predicted that the Pc complexes **3–6** synthesized in this study would exhibit extra solubility in common solvents, minimal aggregation, more red shifted B and Q bands, and a systematic redox shift towards negative potentials in electrochemical measurements compared to their previously studied peripheral analogues [23]. The results we obtained matched exactly with the features we expected. The obtained results were fully consistent with the features of Pcs we expected. Thus, we predict these Pc complexes would perform much superior properties than their peripheral analogues in applications related to electron transfer.

CRediT authorship contribution statement

Efe Baturhan Orman: Electrochemical characterization. **Zuhal Yazar:** Electrochemical characterization. **Mehmet Pişkin:** Synthesis and molecular characterization of macromolecules. **Zafer Odabaş:** Writing – review & editing, Validation, Supervision. **Ali Rıza Özkaya:** Writing – review & editing, Validation, Supervision.

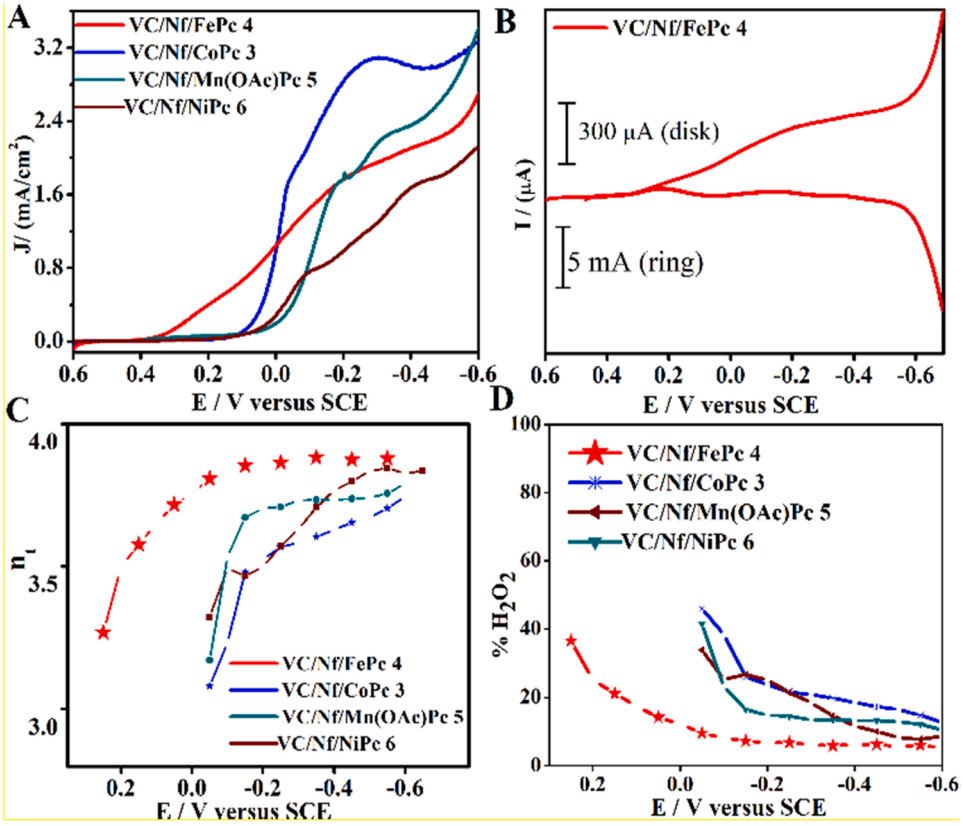

Fig. 10. RDE polarization curves recorded for electrocatalytic ORR with VC/Nf/MPc modified GCEs (A) and RRDE polarization curves recorded for electrocatalytic ORR with VC/Nf/FePc modified GCE (B) in O_2-saturated 0.50 M aqueous H_2SO_4 solution at 2500 rpm. The variation of the number of electrons (C) and the percentage of H_2O_2 (D) with disk potential for VC/Nf/Pc modified electrons (E_{ring} = 0.95 V vs. SCE).

Table 2
Electrocatalytic performances of 3–6 for ORR based on the parameters of limiting diffusion current density (J_L) and the onset potential (E_o).

Complex	[a]E_o / V vs. SCE	[b]J_L / mA cm^{-2}	Ref
FePc **4**	0.350	2.15	tw[c]
CoPc **3**	0.106	3.08	tw[c]
Mn(OAc)Pc **5**	0.010	1.75	tw[c]
NiPc **6**	-0.002	2.48	tw[c]
CoPc	0.100	3.23	[38]
Mn(OAc)Pc	0.030	1.50	[49]
FePc	0.320	4.63	[49]

[a] The potential at which the current density reaches 0.100 mA cm^{-2} was regarded as the onset potential (E_o).
[b] The limiting diffusion current density at 2500 rpm.
[c] This work.

Declaration of Competing Interest

The authors declare that they have no known competing financial interests or personal relationships that could have appeared to influence the work reported in this paper.

Acknowledgments

The authors are gratefully to Scientific Research Projects Committee of Marmara University (BAPKO Project Number: FEN-C-YLP-080715-0345) and Çanakkale Onsekiz Mart University Scientific Research Projects Unit (BAP Project Number: FBA-2018-1225) One of the authors, Ali Rıza Özkaya also thanks Turkish Academy of Sciences (TÜBA) for partial financial support to this study.

Appendix A. Supporting information

Supplementary data associated with this article can be found in the online version at doi:10.1016/j.synthmet.2022.117139.

References

[1] J. Mack, N. Kobayashi, Chem. Rev. 111 (2011) 281–321.
[2] L. Alagna, A. Capobianchi, A.M. Paoletti, G. Pennesi, G. Rossi, M.P. Casaletto, A. Generosi, B. Paci, V.R. Albertini, Thin Solid Films 515 (2006) 2748–2753.
[3] U.E. Ozen, T. Keles, Z. Biyiklioglu, A. Koca, A.R. Ozkaya, J. Electrochem. Soc. 163 (2016) B673–B682.
[4] C. Zhong, M. Zhao, C. Stern, A.G.M. Barrett, B.M. Hoffman, Inorg. Chem. 44 (2005) 8272–8276.
[5] D.C. Chen X, Encyclopedia of Nanoscience and Nanotechnology, American Scientific Publishers, 2004.
[6] A.D. Dinsmore, M.F. Hsu, M.G. Nikolaides, M. Marquez, A.R. Bausch, D.A. Weitz, Science 298 (2002) 1006–1009.
[7] E. Donath, G.B. Sukhorukov, F. Caruso, S.A. Davis, H. Möhwald, Angew. Chem. Int. Ed. 37 (1998) 2201–2205.
[8] Y. Lin, H. Skaff, T. Emrick, A.D. Dinsmore, T.P. Russell, Science 299 (2003) 226–229.
[9] P. Khoza, I. Ndhundhuma, A. Karsten, T. Nyokong, J. Nanosci. Nanotechnol. 20 (2020) 3097–3104.
[10] T. Ceyhan, M.A. Ozdag, B. Salih, M.K. Erbil, A. Elmah, A.R. Ozkaya, O. Bekaroglu, Eur. J. Inorg. Chem. (2008) 4943–4950.
[11] U. Salan, A. Altindal, A.R. Ozkaya, B. Salih, O. Bekaroglu, Dalton Trans. 41 (2012) 5177–5187.
[12] D. Akyuz, R.M.Z. Ayaz, S. Yilmaz, O. Uguz, C. Sarioglu, F. Karaca, A.R. Ozkaya, A. Koca, Int. J. Hydrog. Energ. 44 (2019) 18836–18847.
[13] A. Alemdar, A.R. Ozkaya, M. Bulut, Synth. Met. 160 (2010) 1556–1565.
[14] C.C. Leznoff, A.B.P. Lever, Phthalocyanines: Properties and Applications, VCH, 1989.
[15] M. Harbeck, D.D. Erbahar, I. Gurol, E. Musluoglu, in: 2011 IEEE International Instrumentation and Measurement Technology Conference, 2011, pp. 1–4.
[16] G. Ahumada, Y. Ryu, C.W. Bielawski, Organometallics 39 (2020) 1744–1750.
[17] Z.C. Hern, S.M. Quan, R. Dai, A. Lai, Y. Wang, C. Liu, P.L. Diaconescu, J. Am. Chem. Soc. 143 (2021) 19802–19808.

[18] Z. Zhang, S. Yang, M. Dou, H. Liu, L. Gu, F. Wang, RSC Adv. 6 (2016) 67049–67056.
[19] Z. Zhang, M. Dou, J. Ji, F. Wang, Nano Energy 34 (2017) 338–343.
[20] Q. He, T. Mugadza, G. Hwang, T. Nyokong, Int. J. Electrochem. Sci. 7 (2012) 7045–7064.
[21] A.W. Snow, The Porphyrin Handbook, Academic Press, San Diego, 2003.
[22] J.-D. Wang, M.-J. Lin, S.-F. Wu, Y. Lin, J. Organomet. Chem. 691 (2006) 5074–5076.
[23] E.B. Orman, M. Pişkin, Z. Odabaş, A.R. Özkaya, Electroanalysis 33 (2021) 2310–2322.
[24] R. Li, X. Zhang, P. Zhu, D.K.P. Ng, N. Kobayashi, J. Jiang, Inorg. Chem. 45 (2006) 2327–2334.
[25] T. Kimura, T. Suzuki, Y. Takaguchi, A. Yomogita, T. Wakahara, T. Akasaka, Eur. J. Org. Chem. 2006 (2006) 1262–1270.
[26] M. Pişkin, Polyhedron 104 (2016) 17–24.
[27] N. Nombona, W. Chidawanyika, T. Nyokong, Polyhedron 30 (2011) 654–659.
[28] N. Özgür, I. Nar, A. Gül, E. Hamuryudan, J. Organomet. Chem. 781 (2015) 53–58.
[29] M. Çamur, M. Bulut, J. Organomet. Chem. 695 (2010) 45–52.
[30] S. Altun, E.B. Orman, Z. Odabas, A. Altindal, A.R. Ozkaya, Dalton Trans. 44 (2015) 4341–4354.
[31] S. Altun, Z. Odabas, A. Altindal, A.R. Ozkaya, Dalton Trans. 43 (2014) 7987–7997.
[32] A. Timoumi, M.K.A. Turkestani, S.N. Alamri, H. Alamri, J. Ouerfelli, B. Jamoussi, J. Mater. Sci. Mater. Electron. 28 (2017) 7480–7488.
[33] X. Wenwei, X. Haitao, G. Changsheng, P. Zhongxiao, Y. Tiantang, P. Bixian, Chin. J. Chem. Phys. 16 (2003).
[34] Z. Odabaş, A. Altındal, A.R. Özkaya, M. Bulut, B. Salih, Ö. Bekaroğlu, Polyhedron 26 (2007) 695–707.
[35] J. Janczak, R. Kubiak, M. Śledź, H. Borrmann, Y. Grin, Polyhedron 22 (2003) 2689–2697.
[36] A.J. Bard, L.R. Faulkner. Electrochemical Methods: Fundamentals and Applications, second ed., John Wiley & Sons, Incorporated, 2000.
[37] D. Clack, N. Hush, I. Woolsey, Inorg. Chim. Acta 19 (1976) 129–132.
[38] A. Lever, P. Minor, J. Wilshire, Inorg. Chem. 20 (1981) 2550–2553.
[39] A. Gök, E.B. Orman, Ü. Salan, A.R. Özkaya, M. Bulut, Dyes Pigments 133 (2016) 311–323.
[40] B. Köksoy, O. Soyer, E.B. Orman, A.R. Özkaya, M. Bulut, Dyes Pigments 118 (2015) 166–175.
[41] E.B. Orman, A. Koca, A.R. Ozkaya, I. Gurol, M. Durmus, V. Ahsen, J. Electrochem. Soc. 161 (2014) H422–H429.
[42] M. Çamur, A.R. Özkaya, M. Bulut, Polyhedron 26 (2007) 2638–2646.
[43] N. Saydan, M. Durmus, M.G. Dizge, H. Yaman, A.G. Gurek, E. Antunes, T. Nyokong, V. Ahsen, J. Porphyr. Phthalocyan. 13 (2009) 681–690.
[44] G. Gümrükçü, M.Ü. Özgür, A. Altındal, A.R. Özkaya, B. Salih, Ö. Bekaroğlu, Synth. Met. 161 (2011) 112–123.
[45] M. Özer, A. Altındal, A.R. Özkaya, M. Bulut, Ö. Bekaroğlu, Polyhedron 25 (2006) 3593–3602.
[46] T. Ceyhan, A. Altindal, A.R. Ozkaya, B. Salih, O. Bekaroglu, Dalton Trans. (2009) 10318–10329.
[47] N. Kobayashi, W.A. Nevin, Appl. Organomet. Chem. 10 (1996) 579–590.
[48] N. Sehlotho, T. Nyokong, J. Electroanal. Chem. 595 (2006) 161–167.
[49] D. Akyuz, H. Dincer, A.R. Ozkaya, A. Koca, Int. J. Hydrog. Energ. 40 (2015) 12973–12984.
[50] J.H. Zagal, G.I. Cárdenas-Jirón, J. Electroanal. Chem. 489 (2000) 96–100.
[51] J. Francisco Silva, S. Griveau, C. Richard, J.H. Zagal, F. Bedioui, Electrochem. Commun. 9 (2007) 1629–1634.
[52] E.B. Orman, S. Altun, Z. Odabaş, A. Altındal, A.R. Özkaya, J. Electrochem Soc. 162 (2015) H825–H840.
[53] U.A. Paulus, T.J. Schmidt, H.A. Gasteiger, R.J. Behm, J. Electroanal. Chem. 495 (2001) 134–145.
[54] R.C.M. Jakobs, L.J.J. Janssen, E. Barendrecht, Electrochim. Acta 30 (1985) 1433–1439.
[55] S. Marcotte, D. Villers, N. Guillet, L. Roue, J.P. Dodelet, Electrochim. Acta 50 (2004) 179–188.
[56] M. Lefevre, J.P. Dodelet, Electrochim. Acta 48 (2003) 2749–2760.